Available online at www.sciencedirect.com

ScienceDirect

Materials Today: Proceedings 00 (2014) 000–000

materialstoday: PROCEEDINGS

www.materialstoday.com/proceedings

7th International Symposium on Macro- and Supramolecular Architectures and Materials

Tuning Defects to Facilitate Hydrogen Storage in Core-shell MIL-101(Cr)@UiO-66(Zr) Nanocrystals

Jianwei Ren[a,*], Henrietta W. Langmi[a], Nicholas M. Musyoka[a], Mkhulu Mathe[a], Xiangdong Kang[b], Shijun Liao[c]

[a]*HySA Infrastructure Centre of Competence, Materials Science and Manufacturing, Council for Scientific and Industrial Research (CSIR), PO Box 395, Pretoria 0001, South Africa*

[b]*Shenyang National Laboratory for Materials Science, Institute of Metal Research, Chinese Academy of Sciences, 72 Wenhua Road, Shenyang 110016, China*

[c]*School of Chemistry and Chemical Engineering, South China University of Technology, Wushan Road, Tianhe district, Guangzhou 510640, China*

Abstract

In this work, the existence of structural defects in core-shell MIL-101(Cr)@UiO-66(Zr) and pure UiO-66(Zr) were proposed. It was found that longer synthesis time leads to larger crystals, which are however not perfect as they morphologically appear to be. During the synthesis, the 1,4-benzenedicarboxylic acid (BDC) linker and modulator (HCOOH) may play competitive roles. The modulator employed does not only modulate the crystal growth, but also contributes in the formation of the MOF framework and promotes defects. Although structural defects would facilitate hydrogen storage in MOF structures, they need to be tuned to an optimum level for hydrogen adsorption purpose.

Selection and peer-review under responsibility of the Conference Committee Members of 7th International Symposium on Macro- and Supramolecular Architectures and Materials.

Comment [S1]:

* Corresponding author. Tel.: +27-12-841-2967; fax: +27-12-841-2135.
E-mail address: jren@csir.co.za

Keywords: Structural defects; Metal-organic frameworks; Modulated synthesis; Hydrogen storage;

1. Introduction

Although the presence of porosity in metal-organic framework (MOF) materials confers them interesting properties for potential applications including hydrogen storage [1–5], physical adsorption forces in MOFs are not strong enough to retain small hydrogen molecules due to the low density of H atoms in MOF structures and their fully open pore spaces [6]. Considering this drawback, porosity tailoring has been developed as a strategy to tune pore size and structure in MOFs for an optimal hydrogen uptake at low pressure and ambient temperature [7]. Compared to a non-tailored form of the same framework, this strategy was demonstrated to tune the pore size, achieve higher heat of hydrogen adsorption and enhance the hydrogen uptake [8]. Bai et al. [9–11] and Feng et al. [12] also indicated that MOFs with the coexistence of micro- and mesopore had higher H_2 heat of adsorption for the strong physisorption from inter crystalline mesopores. In our previous study [13], we tailored the porosity by growing UiO-66(Zr) layers onto the surface of seeding MIL-101(Cr), and achieved enhanced hydrogen uptake compared to the individual parent materials. However, we did not straightforwardly identify which factor was responsible for the porosity change. Although a perfect UiO-66 crystal has a 12-connected framework structure (12 BDC linkers), it was recently shown that the real material may contain missing-linker defects, and the hydrogen adsorption behaviors may deviate from those expected for a defect-free crystal [14,15]. As pointed out by Psofogiannakis et al. [16] the diffusion of hydrogen in MOF materials is greatly assisted by structural defects.

In this study, a series of experiments were conducted to understand the effect of growth time on the hydrogen storage performance of core-shell MIL-101(Cr)@UiO-66(Zr) and UiO-66(Zr) nanocrystals. The missing linkers/structural defects-boosted hydrogen storage properties are also discussed.

2. Materials and methods

2.1. Reagents and Chemicals

Zirconium tetrachloride ($ZrCl_4$, Sigma-Aldrich, 99.5+%), chromium chloride hexahydrate ($CrCl_3 \cdot 6H_2O$, Sigma-Aldrich, 99.5+%), terephthalic acid (Sigma-Aldrich, 98%), formic acid (HCOOH, Sigma-Aldrich, 95+%) and N,N-dimethylformamide (DMF, Sigma-Aldrich, 99.8%) were purchased and used without further purification. De-ionized water was obtained from a water purification system (Barnstead Smart2Pure, Thermo Scientific) in the laboratory.

2.2 Preparation of MIL-101, UiO-66 and hybrid MIL-101@UiO-66 nanocrystals

The seeding MIL-101 crystals were prepared by following a previously reported procedure with reaction time of 8 h [17]. The pure UiO-66 sample was synthesized according to another previously reported procedure [18]. The hybrid MIL-101@UiO-66 nanocrystals were prepared as outlined in ref. [13].

2.3 Characterization

X-ray diffraction (XRD) patterns were obtained at room temperature by using a PANalytical X'Pert Pro powder diffractometer with Pixcel detector using Ni-filtered Cu-K_α radiation (0.154 nm) and scanning rate of 0.1 $^\circ \cdot s^{-1}$. An Auriga Cobra focused-ion beam scanning electron microscope (FIB-SEM) was used to study the morphology of the MOF samples. All the samples were mounted on a carbon tape and coated with gold prior to measurement. TEM images were obtained on a JEOL transmission electron microscope (JEM-2100) with an acceleration voltage of 200 kV. The TEM equipped energy dispersive X-ray spectroscopy (EDX) was also employed to determine the composition of the samples.

Thermogravimetric analysis was carried out using a TGA instrument (Netzsch 449C). Before measurements, all the samples were firstly washed by ethanol at 60 $^\circ$C for 2 h, centrifuged off and rinsed using fresh ethanol one more time and dried. The samples were heated up to 800 $^\circ$C at a rate of 5 °C·min^{-1} while exposed to a continuous flow of Ar (30 ml·min^{-1}) on the TGA instrument.

Surface area and pore characteristics measurements were carried out on an ASAP 2020 HD analyzer (Micromeritics) using N_2, and the BET surface areas were obtained from the N_2 isotherms using the two consistency criteria suggested in the literature [19–21]. Hydrogen adsorption isotherms at 77 K and pressure up to 1 bar were

also measured on the ASAP 2020 instrument. All gas sorption isotherms were obtained using ultra-high purity grade (99.999%) gases. Considering that the as-prepared MOF samples may contain free carboxylic acid within the pores [22], before analysis, MOF samples (0.2–0.3 g) were first solvent-exchanged using ethanol, pre-treated in an oven and then outgassed in the analysis tube under vacuum (down to 10^{-7} bar) with heating up to 200 °C, which is sufficient to remove impurities without thermal decomposition or loss of framework crystallinity.

3. Results and discussion

In order to arrive at an optimized formulation for synthesizing the core-shell nanocrystals, the synthesis conditions of MIL-101(Cr) were first optimized. Given the same batch of optimized MIL-101(Cr) seeding crystals, the effect of different growth time of UiO-66(Zr) on the properties of MIL-101(Cr)@UiO-66(Zr) was evaluated.

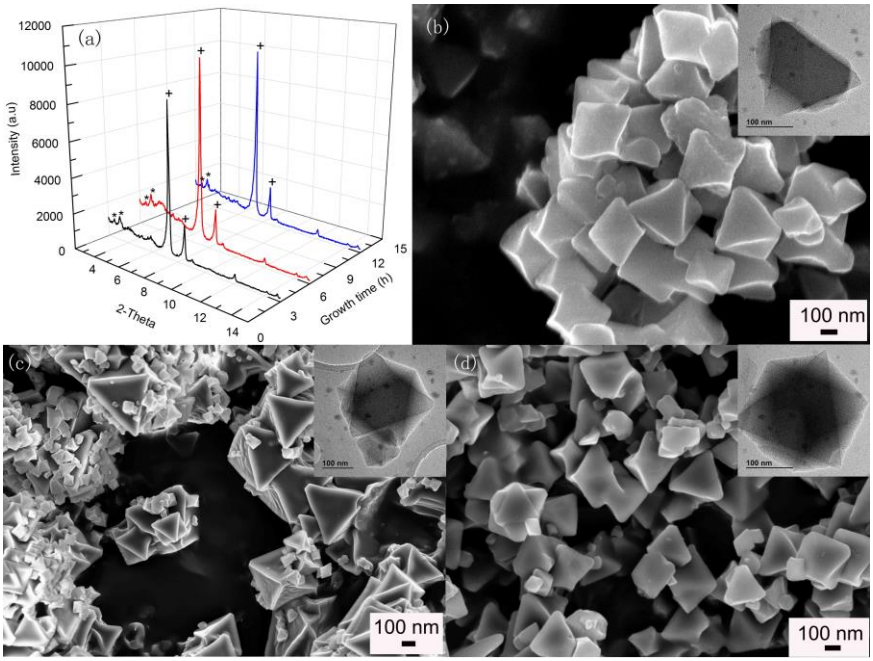

Fig. 1. (a) XRD patterns, and (b-d) SEM images of core-shell MOF (MIL-101(Cr)@UiO-66(Zr) grown for 3, 6 and 12 h, respectively (insert, TEM images).

A direct relationship was noticed between the growth time and the product yield: the longer the growth time the higher the product yield of the core-shell MOF. Fig. 1 presents the XRD patterns and SEM images of core-shell crystals grown for 3, 6 and 12 h, separately. It can be seen that the intensities of the two reflection peaks (2θ = 7.4 and 8.5°, marked with '+') were found to increase with the longer growth time, indicating an increasing content of UiO-66(Zr) in the core-shell MOF. While the intensities of the other two reflection peaks (2θ = 2.8 and 3.3°, marked with '*') relating to the content of MIL-101(Cr) were almost constant. In addition, the SEM image of core-shell sample from 6 h synthesis presents a mixture of small and large nanocrystals. The respective TEM images are inserted and they clearly show the core-shell morphologies. Element analysis indicated the presence of both Cr and Zr elements in the three core-shell samples. The point-and-shoot function from the TEM/EDX was employed to get further evidence on core-shell morphology, the enrichment of Cr element relative to Zr element in the core region, and the enrichment of Zr element in the shell region were detected (Fig. 2).

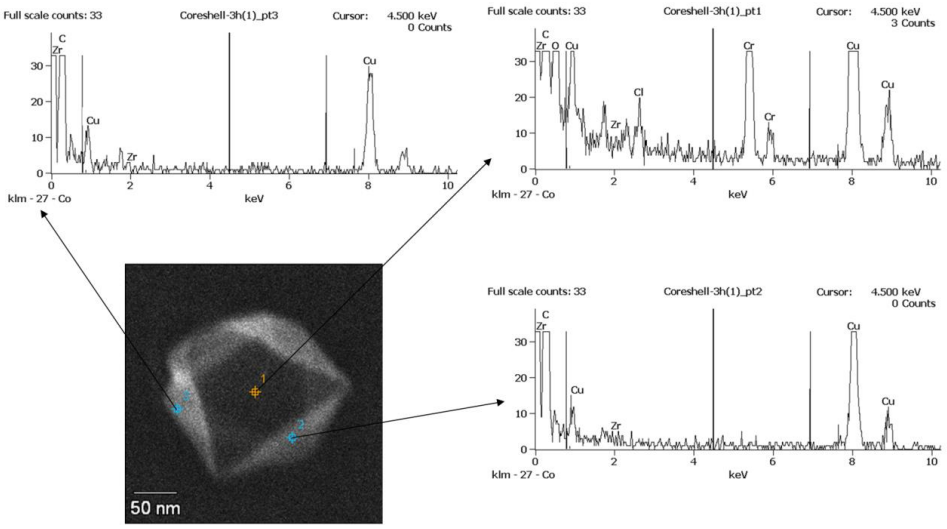

Fig. 2. The TEM/EDX point-and-shoot results from coreshell sample.

Subsequent H_2 sorption measurements indicated that the core-shell samples with longer growth time did not achieve higher hydrogen storage capacities as would have been expected. Given a certain stoichiometric ratio between MIL-101(Cr) and UiO-66 (Zr), the structural defects in UiO-66(Zr) induced by missing linkers may play an important role in hydrogen adsorption, and the diffusion of hydrogen in the MOF materials can be greatly aided by the pore defects. Owing to the above observation, a series of further experiments were conducted to synthesize UiO-66(Zr) samples from different synthesis times of 2, 4, 8, 24, 48 and 72 h (Fig. 3) so as to independently probe the missing linker hypothesis.

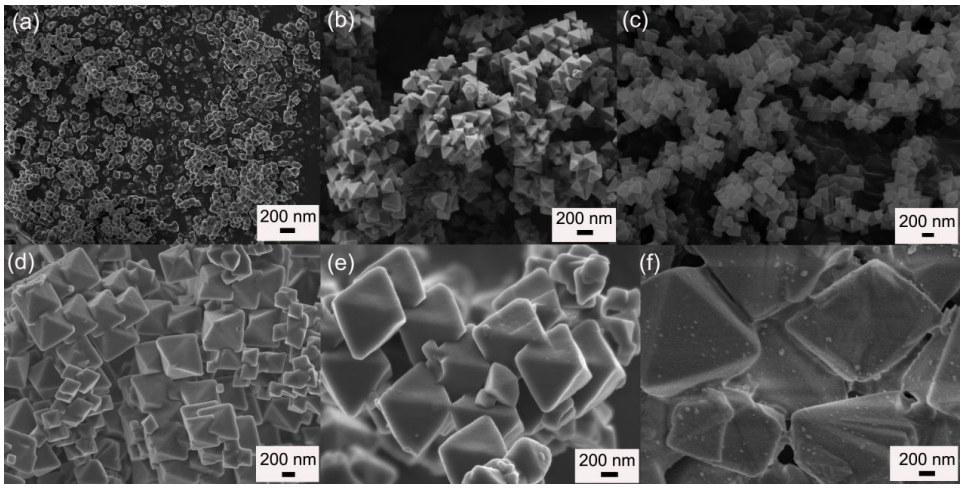

Fig. 3. SEM images of UiO-66 samples, grown for (a) 2 h, (b) 4 h, (c) 8 h, (d) 24 h, (e) 48 h and (f) 72 h.

In the case of UiO-66, it is well established that reacting $ZrCl_4$ with BDC linker precursor leads to intergrown aggregates of small crystallites [23]. Addition of a monocarboxylic acid, such as formic acid, as a modulator enables the crystals to grow into substantially larger sizes with well-defined octahedral shape [23]. The SEM images shown in Fig. 3 allow us to conclude that with increasing synthesis time in a modulated synthesis, the UiO-66 crystals are able to grow into large and well-shaped octahedral crystals.

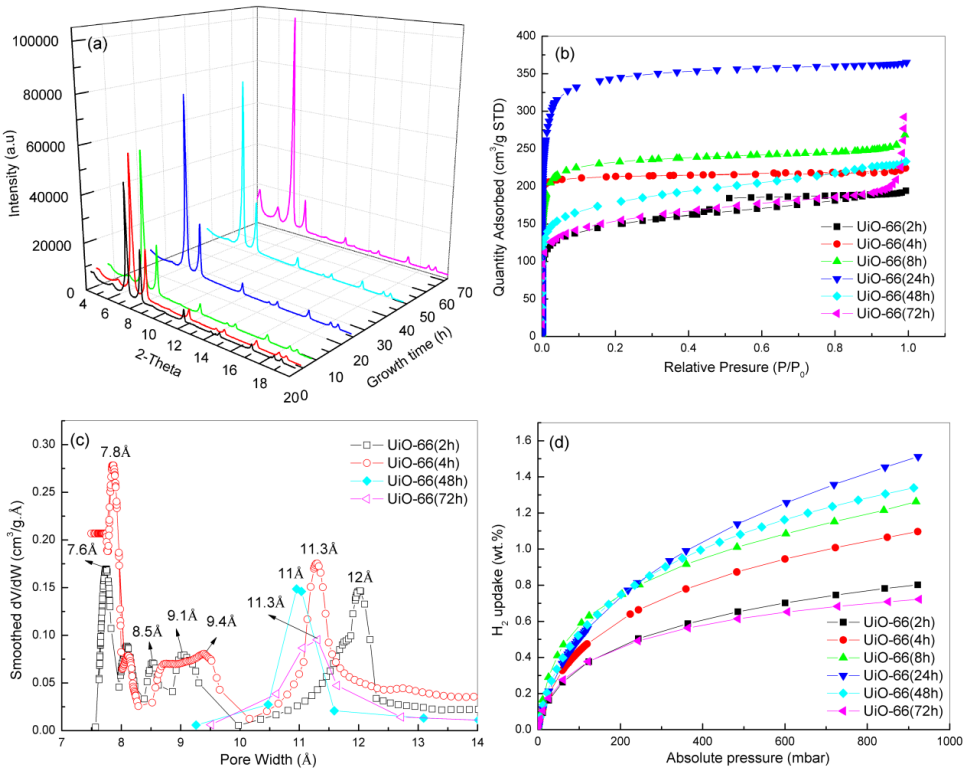

Fig. 4. (a) XRD patterns, (b) N_2 sorption isotherms, (c) pore size distribution and (d) H_2 sorption isotherms.

Fig. 4 shows the XRD patterns, N_2/H_2 sorption isotherms and pore size distribution of UiO-66 samples synthesized using different times of 2, 4, 8, 24, 48 and 72 h. It can be seen from the XRD patterns that longer growth time generally led to higher peak intensities, indicating better crystallinities knowing that XRD in UiO-66 is dominated by heavy element Zr and not sensitive to the organic linkers. The XRD patterns also confirmed that there was no phase transformation happening as the synthesis time was increased. The N_2 sorption isotherm generally indicates longer reaction time resulted in the deviation of the expected trend of the isotherms. The pore size distribution curves in Fig. 4c give evidence of pore size shifting to larger diameters. In fact, for a defect-free UiO-66 crystal with composition, $Zr_6O_4(OH)_4(BDC)_6$, the theoretical pore volume, BET and Langmuir surface area are moderate: 0.4 $cm^3 \cdot g^{-1,}$ 954 and 1187 $m^2 \cdot g^{-1}$, respectively [24]. Considering a hypothetical model structure with ordered defects, in this case a crystal where one of the 12 linkers has been artificially removed for every metal centre in the unit cell, the calculated pore volume and BET surface area are substantially higher: 0.5 $cm^3 \cdot g^{-1}$ and 1433 $m^2 \cdot g^{-1}$, respectively [24]. The presence of structural defects within UiO-66 can explain the relevant findings that the experimental values of BET are larger than calculated ones [25]. This makes sense considering the

hypothesis that linker deficiencies induce a porous framework though the presence of too many defects may have adverse effects on the porosity.

The N_2/H_2 sorption isotherms are consistent with pore size distribution curves, which show an increasing pore size with increasing contact time of reactants with the formic acid modulator. This also implies that the apparently larger crystals with well-defined octahedral shapes are not as structurally perfect as they seem to be. As indicated by Wu et al. [24] the role of the modulator used in Zr-MOF synthesis is not only to modulate the crystal growth, but it also participates in the framework formation and promoting defects. However, this is not the case for the modulated synthesis of HKUST-1, where the modulator employed did not induce significant defects within the framework [26]. This is unsurprising due to the instability of the missing-linker defects in MOFs with low network connections such as HKUST-1. Table 1 compares the physical properties and H_2 uptake capacities of the obtained UiO-66 samples. As the synthesis time increased, the crystal size, surface area and pore volume increased up to synthesis time of 24 h. After this time, the surface area and pore volume decreased. In fact, the UiO-66 sample with much longer synthesis time of 72 h displayed lower BET surface area and pore volume than the defect-free UiO-66. This indicates that there may be a competitive role between BDC linkers and HCOOH modulator, and the creation of too many defects would lower the BET surface area and pore volume, resulting in lower hydrogen storage capacities.

Table 1. Comparison of physical properties and H_2 uptake capacities of the obtained UiO-66(Zr) samples

Sample	Size[a]	S^b_{BET} $(m^2 \cdot g^{-1})^b$	$S^c_{Langmuir}$ $(m^2 \cdot g^{-1})^c$	Pore vol[d]. $(cm^3 \cdot g^{-1})^d$	Micro. vol[e]. $(cm^3 \cdot g^{-1})^e$	H_2 uptake[f] (wt.%)[f]
UiO-66 (2h)	100 nm	940	1180	0.41	0.36	0.8
UiO-66 (4h)	150 nm	1087	1294	0.44	0.38	1.1
UiO-66 (8h)	200 nm	1137	1355	0.48	0.40	1.3
UiO-66 (24h)	1–3 μm	1367	1578	0.56	0.44	1.5
UiO-66 (48h)	1–3 μm	1258	1376	0.51	0.36	1.4
UiO-66 (72h)	1–3 μm	559	669	0.46	0.14	0.7
Defect-free UiO-66 [24]	/	954	1187	0.43	/	/

[a]Estimated from SEM images. [b]BET surface area. [c]Langmuir surface area. [d]From H-K analysis. [e]From H-K analysis. [f]Absorbed at 77 K up to 1 bar.

Several approaches have been undertaken to identify the structural defects within UiO-66, such as the presence of symmetry forbidden reflections in PXRD patterns [27], less weight loss than expected during thermal decomposition [28], higher surface area and pore volume than theoretically expected [29], more O-H stretching bands from FTIR spectrum [30], unexpected split and weakened fingerprints in Raman spectrum [31]. In line with the weight loss approach, thermogravimetric analysis (TGA) has been employed to identify MOF structural defects [32–34]. UiO-66 is well known as the prototypical Zr-MOF with a face-centred cubic crystal structure. The Zr ion is linked by eight oxygen in the as-synthesized material, and six of them cluster together, to form the $Zr_6O_4(OH)_4$ metal centre. Each Zr metal centre is linked to 12 BDC linkers to form the 3D framework (hydroxylated form). Upon heating at high temperature (~200 °C) in vacuum, two H_2O molecules per Zr-O cluster are lost, reducing the Zr-O coordination to 7 (dehydroxylated form) [35,36]. In this work, in order to evaluate the absence of linkers connecting the inorganic units, the last part of the TGA curves for samples synthesized from different synthesis times were compared (Fig. 5). For defective UiO-66, there would usually be a higher mass loss than expected which would arise from structural decomposition between 300–650 °C.

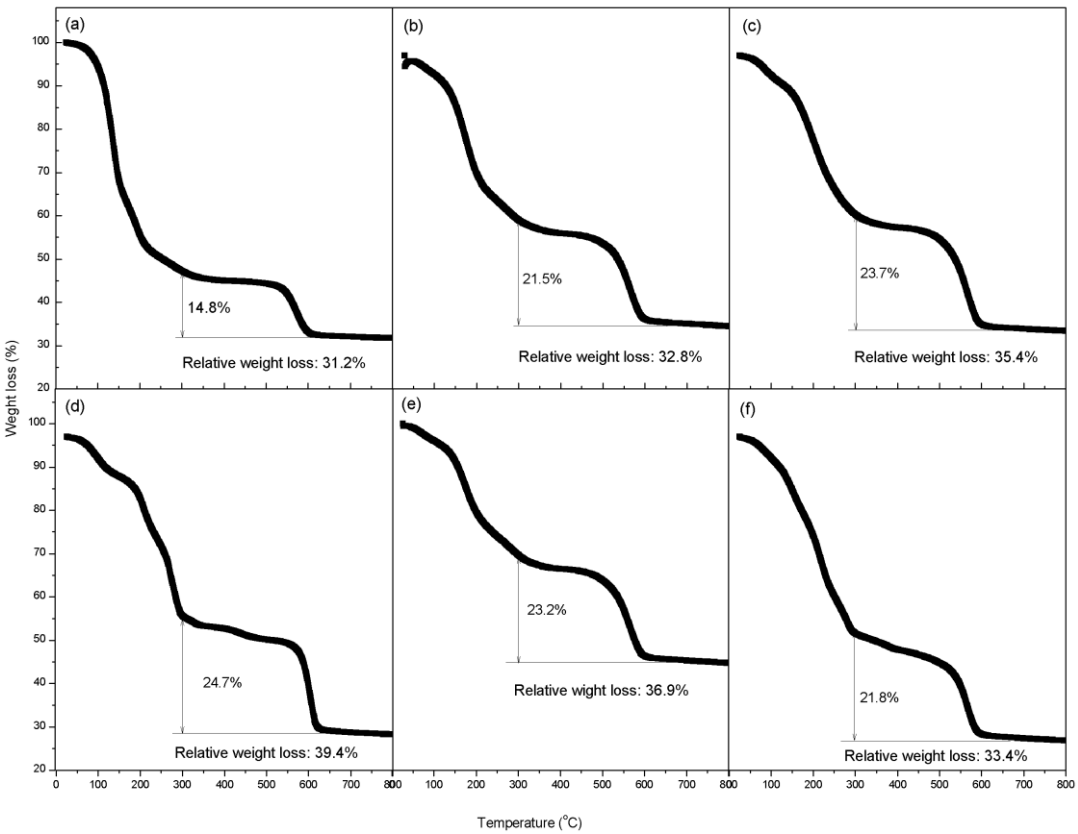

Fig. 5. TG curves of UiO-66 samples grown for: (a) 2 h, (b) 4 h, (c) 8 h, (d) 24 h, (e) 48 h and (f) 72 h.

The mass at 300 °C was considered as the dry mass for all the UiO-66 samples. As can be seen in Fig. 5, this corresponds to a point after the initial mass losses due to the dehydration and desolvation of the materials. During TGA measurements, both the physisorbed water molecules and solvent molecules cannot be precisely defined stoichiometrically, but the loss of benzene ring can be distinctively defined [37]. The plateau in the 300–650 °C range of TGA plots in Fig. 5 signifies the chemical formula, $ZrO(CO_2)(C_6H_4)$, per Zr atom. The mass difference in this range is considered as the mass loss due to the decomposition of the materials and the formation of ZrO_2, since after 650 °C the mass becomes constant for all samples. For UiO-66, a theoretical mass loss of 54.6 % relative to the mass at 300 °C should be obtained at the end, assuming the decomposition of the BDC linkers. For UiO-66 samples from 2, 4, 8 and 24 h synthesis, the relative weight losses are 31.2, 32.8, 35.4 and 39.4 %, indicating an increasing content of linkers per unit. As mentioned earlier, for these samples, the BET surface area, pore volumes and hydrogen storage capacities increased. Meanwhile when the synthesis time was increased to 48 and 72 h, the BET surface areas, pore volumes and hydrogen storage capacities of the obtained samples dropped. Considering that the BDC linkers and HCOOH play competitive roles, there is a need to find an optimized condition for a certain synthesis. In this way, the concept of 'defects-engineering' can then be introduced.

4. Conclusion

In this work, the effect of structural defects in core-shell MIL-101(Cr)@UiO-66(Zr) and particularly pure UiO-66(Zr) on BET surface area, pore volume and hydrogen adsorption properties was investigated. It was shown that the longer synthesis time of UiO-66 resulted in larger crystals, which were apparently not perfect as they morphologically seemed to be. During the synthesis, the BDC linker and HCOOH modulator may play competitive roles. The modulator utilized here is not only modulating the crystal growth, but also partaking in the MOF framework formation and engaging in the generation of defects. Structural defects would facilitate the diffusion of hydrogen into MOF materials. Nevertheless, these defects need to be properly tuned to an optimum state for use in hydrogen storage.

Acknowledgements

This work was financially supported by the South African Department of Science and Technology (DST) for the HySA Infrastructure (Grant No. HTC004X), the National Research Foundation (NRF) for the South Africa/China research collaboration grant (Grant No. HTC059X), DST-NRF Professional Development Programme (PDP) (Grant No. HTC063X) and the CSIR-Young Researcher Establishment Fund (Grant No. HTC066P).

References

[1] M.P. Suh, H.J. Park, T.K. Prasad, D.W. Lim, Chem. Rev. 112 (2012) 782–835.

[2] T. Hügle, M. Hartl, D. Lentz, Chem. Eur. J. 7 (2011) 10184–10207.

[3] D.J. Durbin, C. Malardier-Jugroot, Int. J. Hydrogen Energy 38 (2013) 14595–14617.

[4] J.S. Xiao, M. Hu, P. Bénard, R. Chahine, Int. J. Hydrogen Energy 38 (2013) 13000–13010.

[5] S.L. James, Chem. Soc. Rev. 32 (2003) 276–288.

[6] M. Felderhoff, C. Weidenthaler, R. von Helmolt, U. Eberle, Phys. Chem. Chem. Phys. 9 (2007) 2643–2653.

[7] H. Frost, R.Q. Snurr, J. Phys. Chem. C 111 (2007) 18794–18803.

[8] T.B. Lee, D.H. Jung, D. Kim, J. Kim, K. Choi, S.H. Choi, Catal. Today 146 (2009) 216–222.

[9] A. Xin, J. Bai, Y. Pan, M.J. Zaworotko, Chem. Eur. J. 16 (2010) 13049–13052.

[10] Z. Xin, J. Bai, Y. Shen, Y. Pan, Cryst. Growth Des. 10 (2010) 2451–2454.

[11] H. Du, J. Bai, C. Zuo, Z. Xin, J. Hu, CrystEngComm 13 (2011) 3314–3316.

[12] Y.F. Feng, H. Jiang, M. Chen, Y.R. Wang, Powder Technol. 249 (2013) 38–42.

[13] J.W. Ren, N.M. Musyoka, H.W. Langmi, B.C. Brian, M. Mathe, X.D. Kang, Int. J. Hydrogen Energy 39 (2014) 14912–14917.

[14] Q.Y. Yang, A.D. Wiersum, H. Jobie, V. Guillerm, C. Serre, P.L. Llewellyn, G. Manrim, J. Phys. Chem. C 115 (2011) 13768–13774.

[15] R. Ameloot, F. Vermoortele, J. Hofkens, F.C. De Scheyver, D.E. De Ves, M.B.J. Roeffaers, Angew. Chem. Int. Ed. 52 (2013) 401–405.

[16] G.M. Psofogiannakis, G.E. Froudakis, J. Phys. Chem. C 115 (2011) 4047–4053.

[17] J.W. Ren, N.M. Musyoka, H.W. Langmi, T. Segakweng, B.C. North, M. Mathe, X.D. Kang, Int. J. Hydrogen Energy 39 (2014) 12018–12023.

[18] J.W. Ren, H.W. Langmi, B.C. North, M. Mathe, D. Bessarabov, Int. J. Hydrogen Energy 39 (2014) 890–895.

[19] J. Rouquerol, P. Llewellyn, F. Rouquerol, Stud. Surf. Sci. Catal. 160 (2007) 49–56.

[20] Y.S. Bae, A.Ö. Yazayd'n, R.Q. Snurr, Langmuir 26 (2010) 5475–5483.

[21] K.S. Walton, R.Q. Snurr, J. Am. Chem. Soc. 129 (2007) 8552–8556.

[22] A. Vimont, J.M. Goupil, J.C. Lavalley, M. Daturi, S. Surblé, C. Serre, F. Millange, G. Férey, N. Audebrand, J. Am. Chem. Soc. 128 (2006) 3218–3227.

[23] A. Schaate, P. Roy, A. Godt, J. Lippke, F. Waltz, M. Wiebcke, P. Behrens, Chem. Eur. J. 17 (2011) 6643–6651.

[24] H. Wu, Y.S. Chua, V. Krungleviciute, M. Tyagi, P. Chen, T. Yildirim, W. Zhou, J. Am. Chem. Soc. 135 (2013) 10525–10532.

[25] G.E. Cmarik, M. Kim, S.M. Cohen, K.S. Walton, Langmuir 28 (2012) 15606–15613.

[26] S. Diring, S. Furukawa, Y. Takashima, T. Tsuruoka, S. Kitagawa, Chem. Mater. 22 (2010) 4531–4538.

[27] S. Jakobsen, D. Gianolio, D.S. Wragg, M.H. Nilsen, H. Emerich, S. Bordiga, C. Lamberti, U. Olsbye, M. Tilset, K.P. Lillerud, Phys. Rev. B 86 (2012) 125429–125440.

[28] M.L. Pinto, S. Dias, J Pires, ACS Appl. Mater. Interfaces 5 (2013) 2360–2363.

[29] M.J. Katz, Z.J. Brown, Y.J. Colon, P.W. Siu, K.A. Scheidt, R.Q. Snurr, J.T. Hupp, O.K. Farha, Chem. Commun. 49 (2013) 9449–9451.

[30] G.C. Shearer, S. Forselv, S. Chavan, S. Bordiga, K. Mathisen, M. Bjørgen, S. Svelle, K.P. Lillerud, Top Catal. 56 (2013) 770–782.

[31] G.C. Shearer, S. Chavan, J. Ethiraj, J.G. Vitillo, S. Svelle, U. Olsbye, C. Lamberti, S. Bordiga, K.P. Lillerud, Chem. Mater. 26 (2014) 4068–4071.

[32] S. Øien, D. Wragg, H. Reinsch, S. Svelle, S. Bordiga, C. Lamberti, K.P. Lillerud, Cryst. Growth. Des. 14 (2014) 5370–5372.

[33] O. Kozachuk, M. Meilikhov, K. Yusenko, A. Schneemann, B. Jee, A.V. Kuttatheyil, M. Bertmer, C. Sternemann, A. Pöppl, R.A. Fischer, Eur. J. Inorg. Chem. 26 (2013) 4544–4557.

[34] M. Vandichel, J. Hajek, F. Vermoortele, M. Waroquier, D.E. Devos, V.V. Speybroeck, CrystEngComm. 2015, in press. DOI: 10.1039/C4CE01672F.

[35] J.H. Cavka, S. Jakobsen, U. Olsbye, N. Guillou, C. Lamberti, S. Bordiga, K.P. Lillerud, J. Am. Chem. Soc. 130 (2008) 13850–13851.

[36] H. Wu, T. Yildirim, W. Zhou, J. Phys. Chem. Let. 4 (2013) 925–930.

[37] L. Valenzano, B. Civalleri, S. Chavan, S. Bordiga, M.H. Nilsen, S. Jakobsen, K.P. Lillerud, C. Lamberti, Chem. Mater. 23 (2011) 1700–1718.